Optimised Design of Nested Oblong Tube Energy Absorbers under Lateral Impact Loading.

A.G. Olabi[a] *, E. Morris[a], M.S.J. Hashmi[a], and M.D. Gilchrist[b]

* Email: abdul.olabi@dcu.ie

a School of Mechanical and Manufacturing Engineering, Dublin City University, Glasnevin, Dublin 9, Ireland.

b School of Electrical, Electronic and Mechanical Engineering, University College Dublin, Belfield, Dublin 4, Ireland.

Abstract.

Dynamic lateral crushing of mild steel (DIN 2393) nested tube systems was conducted using a ZWICK ROELL impact tester. The tests were performed with impact velocities ranging between 3 and 5 m/s, achieved using a fixed mass impinging onto the specimens under the influence of gravity. The various nested tube systems consisted of one standard and one optimised design. Their crushing behaviour and energy absorption capabilities were obtained and analysed.

In addition to the experimental work, numerical simulations using the explicit code LS-DYNA were conducted; boundary conditions matching those observed in experiments were applied to the models. Results from the numerical method were compared against those obtained from experiments. An over-prediction in force-deflection responses was obtained from the numerical code. An attempt was made to explain this inconsistency on the basis of the formation of plastic hinges and the validity of strain rate parameters used in the Cowper Symonds relation. It was found that the optimised energy absorbers exhibited a more desirable force-deflection response than their standard counterparts due to a simple design modification which was incorporated in the optimised design.

Nomenclature.

OIPSS Oblong In Plane Standard System

OIPDS Oblong In Plane Damped System

CIPDS Circular In Plane Damped System

$\dot{\varepsilon}$ Strain rate

σ_d Dynamic yield stress.

σ_s Static yield stress

D, q Strain rate parameters (Cowper-Symonds relation)

E_{kin} kinetic energy

E_{int} internal energy

E_{si} sliding energy (friction energy)

E_{rw} rigid wall energy

E_{damp} damping energy

E_{hg} hourglass energy

E_{kin}^{0} Initial kinetic energy

E_{int}^{0} Initial internal energy

E_{ext} External work done

1.0 Introduction.

The function of an energy absorber is to absorb kinetic energy upon impact and dissipate it in some other form of energy, ideally in an irreversible manner. Non-recoverable (inelastic) energy can exist in various forms such as plastic deformation, viscous energy and friction or fracture energy. Circular or square sectioned tubes are one of the most commonly used structural elements due to their prevalent occurrence and easy manufacturability. Circular tubes, for example, can dissipate elastic and inelastic energy through different modes of deformation, resulting in different energy absorption responses. Such methods of deformation include lateral compression, lateral indentation, axial crushing, tube splitting and tube inversion. It is important to study their energy absorption characteristics and mean crushing loads so as to determine their applicability to practical energy absorption situations. Such practical cases may consist of energy absorbers in the aircraft, automobile and spacecraft industries, nuclear reactors, steel silos and tanks for the safe transportation of solids and liquids.

Energy absorption through material deformation has been extensively studied over the last three decades, particularly in the form of tubular systems. The lateral compression of a single circular tube and its strain hardening phenomena have been analysed both experimentally and analytically by various authors such as Burton and Craig [1], DeRuntz and Hodge [2], and Redwood [3]. These authors were among the first to analyse such problems and each one of them proposed a slightly different deformation mechanism for the compression of a tube between rigid flat platens. The effect of strain hardening was further examined by Reid and Reddy [4] who developed a theoretical model based on a rigid linearly strain hardening material model which appears to be the most accurate one to date. The authors improved the strain hardening prediction by replacing the localised hinges with an arc in which its length changes with deflection. Hence this theoretical model accounted for both the geometric and material strain hardening effect. An important dimensionless parameter which was developed governs the shape of the force-deflection curve. This parameter is defined as 'mR' and is a function of the yield stress in tension, the mean radius R of the tube, the strain hardening modulus E_p and the thickness t. According to Reid and Reddy it may be possible to maximise the energy absorbing capacity by choosing appropriate tube dimensions such that the 'mR' value is minimised since this is a function of tube geometry. Avalle and Goglio [5] examined the strain field generated during the lateral compression of aluminium tubes and proceeded to verify the known theoretical models. Of the three known theoretical models proposed by the various authors [1, 2, 3], it was found that the latter accounted for all the main features observed

experimentally, hence this model seems the most realistic in describing the actual behaviour of the tube both qualitatively and quantitatively. Reddy and Reid [6] proposed a method to calculate a more realistic force-deflection curve using a rigid linear work hardening material model. These tubes were also compressed laterally between rigid platens. It was suggested that an average value of strain hardening modulus could be used to calculate the parameter *'mR'*, therefore these two parameters would be considered constant throughout the deflection range. However, it has been further proposed that if the variation of strain hardening modulus with strain is identified, this could be used to update *'mR'* at each load step or load increment and thus obtain a more realistic load-deflection characteristic. It was suggested that the method described above could be used as a basis for obtaining some of the material properties from a ring compression test. Gupta et al [7] conducted a comprehensive experimental and computational investigation of circular metallic tubes subjected to quasi-static lateral loading. Specimens analysed consisted of both mild steel and aluminium tubes with different diameter to thickness ratios. Their corresponding force-deflection responses were obtained and examined in detail. An in depth description was provided on the deformation mechanism of a tube compressed between flat rigid platens. Nested systems in the form of a line of rings subjected to end impact loading were examined by Reid and Reddy [8]. The authors were principally concerned with identifying the main mechanism which controls the deformation of such systems. Upon experimentation, the main parameters were identified and varied, thereby leading to a suggestion for the construction of a mathematical model of the system. It was found that in low speed impact testing on tube systems, the effect of inertia was secondary; therefore the design of energy absorbing systems could be achieved provided that the material strain rate was taken into account. Reddy et al [9] described experiments in which a variety of one dimensional systems with free distal ends, as opposed to fixed ends, were subjected to lateral impact by a rigid projectile. An elastic–plastic structural shock wave theory, which employs a bilinear material model to describe the collapse behaviour of the rings, was used to analyse the deformation of typical ring chain systems.

A nested system in the form of orthogonal layers of aluminium and mild steel tubes under static lateral compression was investigated by Johnson et al [10]. Such an orthogonal layer consists of a row of tubes stacked upon each other with every second row rotated 90 degrees. The authors concluded that nested ductile tube systems play an important part in producing a monotonic load-deflection response and that the systems which exhibit cracks after loading only induce oscillations into the response and do not produce catastrophic failure in the system as a whole.

A nested system analysed by Shrive et al [11] consisted of two concentric rings with a layer of smaller tubes between them, the axis of all tubes been parallel. Tack welding was used to attach the rings to the concentric tubes. It was found that increases in system stiffness, maximum load and energy absorption was apparent as the level of tack welding increased. From the impact loading experiment, it was found that full deformation did not occur but maximum opposing forces similar to the quasi-static case were achieved.

Reddy [12] examined both theoretically and experimentally the quasi-static lateral compression of a tube constrained so that its horizontal diameter was prevented from increasing. This was a way of increasing the specific energy absorption capacity of the tube by introducing more plastic hinges into the structure. Also the relationship between a single tube and a system of tubes with different configurations was investigated. It was found that the energy absorbed by a closed system (side constraints) was three times more than that of an open system (no constraints); however the maximum deflection of the former was less than that of an open system. Overall it can be concluded that the introduction of side constraints and creating a closed system is a feasible method of increasing its energy absorbing efficiency.

Morris et al [13] analysed the quasi-static lateral compression of nested tube systems between rigid platens both experimentally and numerically. These energy absorbers consisted of both two and three tube systems which were assembled ‘In Plane’. Such a term describes two or more tubes of varying diameter being placed within each other and their axes being parallel. This type of energy absorber was compressed under flat rigid platens at a velocity of 3mm/min to ensure no dynamic effects were present. It was demonstrated how such a system is well suited to applications where space or volume restrictions are an important design consideration without compromising energy absorbing requirements.

Morris et al [14] also analysed the post collapse response of nested tube systems with side constraints. This work showed how the introduction of external constraints allows a greater volume of material within the structure to deform plastically in the post collapse stage of compression, thereby absorbing more energy. Nested systems consist of ‘short tubes’ of varying diameter placed within each other with an eccentric configuration. Both experimental and computational techniques were used to analyse the quasi-static response of such systems. Numerical results generated were found to be in good agreement with those of experiment. A related work [15] modified the ‘In Plane’ system by rotating the central tube ninety degrees to define an ‘Out of Plane System’. In doing so, the force-deflection response changed from a non-monotonically increasing response to one that increased monotonically without sacrificing its

energy absorbing capabilities. The quasi-static lateral compression was achieved using three different devices such as flat rigid platens, cylindrical and point-load indenters and their corresponding force-deflection response were compared.

Morris et al [16] also studied nested tubes crushed laterally between rigid platens at two different velocities. The first category of energy absorber consisted of an 'In Plane' system; the second device consisted of an 'Out of Plane' system. Material used was cold finished, drawn over mandrel (DIN 2393 ST 37-2) mild steel. The Cowper-Symonds relation was used to predict the dynamic yield stress of the rings and this was included in the FE material model.

Reid et al [17] experimentally analysed the energy absorbing capacity and collapse mechanism of braced metal tubes compressed under rigid platens. Their aim was to design an energy absorber to cope with both the 'redirectional' and 'trapping' of vehicles involved in side impacts. 'Redirectional' is a term used to describe where the vehicle moved back onto its original line of travel after the collision has occurred. 'Trapping' involves catching the vehicle so as to prevent the probability of secondary conflicts occurring with oncoming traffic. They conducted initial investigations on small scale components to explore the possibility of achieving the desired response by introducing tension members across the diameters of the mild steel tubes in question. Both single and double braced tubes of various angles were analysed. They stated that the response of a braced tube, whether singly or doubly, is sensitive to the direction of loading, however; significant enhancement in the energy absorbing capacity of such systems can be achieved. Full scale testing was also carried out on the double braced tubes used as a cluster in a modular crash cushion.

Wu and Carney [18] analytically analysed the initial collapse of braced elliptical tubes under later compression. Elliptical tubes provide a distinct advantage over their original circular tube counterparts in that the crush efficiency is greater. This automatically implies that the specific energy absorbing capacity of such devices increases, which is desirable in the design of impact attenuation devices. Another method of increasing the specific energy absorbing capacity of these cylindrical or elliptical devices is through the inclusion of metallic braces or wire. These can be attached to the devices either horizontally or at an angle. This generates a larger collapse load and hence the specific energy absorbing capacity is increased. Three possible collapse mechanisms for braced circular tubes as established by Reid [17] have also been found to exist for braced elliptical tubes. These three cases are tubes with small bracing angles, tubes with horizontal bracing and tubes with large bracing angles. It was found that the initial collapse load of braced elliptical tubes was dependant on both the ratio of the ellipse axes b/a, and the bracing angle. ABAQUS, a

finite element software was used to capture the deformation mechanisms and initial collapse load of the devices.

In a companion paper Wu and [19], the same authors presented the experimental results of braced elliptical tubes compressed under rigid platens. This was to authenticate the numerical and theoretical results presented in their initial paper. It was found that for a ratio of b/a = 1 (Circular tubes), the initial collapse loads predicted from the EST method (Equivalent Structure Technique), ABAQUS and experiments were comparable particularly for small-angle braced tubes. However, for large brace angles, the experimental results are below theoretical predictions and according to the author are due to the tubes being highly sensitive to geometrical imperfections. Finally, it was noted that the ABAQUS results were much lower than the results predicted by the EST method and this appears to be due to the omission of membrane stresses in the latter case.

It can be seen that extensive research has been conducted by the aforementioned authors in the study of both singular tubes and externally stacked nested systems subjected to lateral loading. However it appears that no investigation has been conducted on the dynamic crushing of an internally stacked system in which a cluster of tubes are assembled as described by Morris [13]. The lateral crushing of nested oblong tubes provides a distinct advantage over their circular counterparts in that a greater lateral displacement stroke can be achieved and hence, the specific energy absorbing capacity increases for such systems. Therefore, this paper is an attempt to consider the effectiveness of this new form of nested system as an energy absorber. In addition, the paper demonstrates how such systems can be optimised so that a desirable force – deflection response can be obtained by introducing a simple mechanism. Experimental analysis of these devices was achieved with the aid of a drop weight impact tester. The loading and response was analysed via the finite element method and the predicted force-deflection response was compared against that measured experimentally.

2.0 Experimental Set-up.

2.1 High Speed Camera.

A high speed video recording system namely the MOTIONSCOPE PCI 2000 S series was used to capture each impact event. The camera head is a 2 ½ * 2 ½ * 4 inch enclosure which contains the CCD sensor. Up to 2000 fps (frame per seconds) of the impact event can be recorded. Video playbacks of 2000 fps in forward and reverse directions are also possible with frame by frame or freeze frame options available. The exposure of each frame is reduced at the higher frame rates, so more light exposure is required as the

frame rate increases. Therefore a specialised lighting system was employed to increase illumination. The video files are in Microsoft avi (audio video interleaved) format by default; however they can be converted to jpeg with resolutions of up to 480*420 pixels depending on the number of fps used.

2.2 Mechanical Features of the Impact Tester.

A Kistler 9091 series piezoelectric force transducer was used to capture the load-time response of the impact events. This transducer has a large dynamic range and good frequency responses of 160,000 samples/sec. Maximum load magnitudes of up to 250kN are possible. The transducer is placed in the moving carriage and connected to the striker via a lock-unlock mechanism. The complete moving mass consisting of both the carriage and striker is allowed to drop vertically between 2 vertical sliding guide rails from a maximum height of 1.2 metres.

A photo gate arrangement consisting of photo diodes which pass through a flagged gate was used to capture the initial velocity of the striker just before impact.

2.3 Data Acquisition System.

The data acquisition system Rosand IFW (Intelligent Free Wheel) V 1.10 was used to capture the signals from the force transducer. The software gathers the force measurements with respect to time, the frequency of which is dependent on sweep time and number of data points selected. The maximum sampling rate is 670 KHz. If the signal filter is used, then the data is shown with a filter applied but this can be applied or removed retrospectively as raw data is always stored. The type of filter used is based on the second order Butterworth filter, implemented in the software as an IIR (infinite impulse response), i.e. a recursive filter.

2.4 Material Properties.

The tubes used in this work were made of mild steel which was cold finished, drawn over mandrel by the tube manufacturer according to DIN standards (DIN 2393 ST 37.2) and containing approximately 0.15% carbon. The three tubes used in each energy absorber were of 127mm O.D., 101.6mm O.D. and 76.2mm O.D. respectively with the thickness of each being 3.25mm. The length of the tubes within the two systems analysed in this work, namely the OIPSS and the OIPDS, are of 10mm and 15mm respectively. Three to four tensile samples for each of the three different sized tubes were analysed in order to ensure consistent results. The dog bone samples were machined from cut-out specimens obtained from the

acquired tube stock. The true static stress-strain curve was obtained using a tensile test based on ASTM standards and are displayed in Fig. 1a. Since the tubes were cold worked by the tube manufacturer, the true stress - strain curves obtained from the samples exhibited a deformation characteristic in which necking occurred immediately after yielding followed by a geometrical softening stage. This is to be expected since the cold rolling process, in addition to increasing the yield strength, decreases the ductility due to the concentrated dislocations in the material. Such behaviour is termed tension instability and hence Considère's criterion can be employed to determine the initial plastic stiffness of the material. This criterion states that $\sigma = d\sigma / d\varepsilon$, implying that the initial plastic modulus must be less than or equal to the yield stress. Therefore, it was decided to approximate the material property of the three tubes using a bilinear stress-strain curve. In doing so, the yield stress of 470MPa was carefully obtained from the experimental true stress-strain curve and according to Considère's criterion; the initial plastic modulus was assigned the same value of 470MPa. The yield stress is validated according to DIN standards which state the yield stress of this material to be within the range of 450 MPa to 525MPa.

3.0 Experimental Work.

3.1 The Preparation Stages.

For the impact testing of the samples, a Zwick Roell version 5HV was employed as shown in Fig. 2a. A custom made fixture was designed and manufactured to hold the samples relative to the impinging striker as shown in Fig. 2b. It should be noted that such a fixture will automatically prevent the full displacement stroke to be achieved; approximately 5mm of a displacement stroke is lost. Fig. 2c illustrates a schematic of both the OIPSS (Oblong In-Plane Standard System) and the OIPDS (Oblong In-Plane Damped System). A slight difference exists between both systems in that the OIPDS consist of a simple mechanism, its function which is to cause all three tubes to deform synchronously when loaded dynamically by the impinging striker. This synchronous movement of the three tubes enables a desirable rectangular force-deflection response to be achieved which is explained at a later stage. A total of ten samples were tested as shown in Table 1. This table displays their corresponding initial velocity, final velocity, impact duration, displacement and energy absorbed. For the testing of each sample, the impinging mass was kept at a constant value of 34.7kg. This total mass consisted of both the striker and the carriage. The machine allows the user to select one of three parameters to set the striker in motion. These parameters consist of velocity, drop height and energy absorption. The latter option was used and hence the corresponding velocity and drop height were calculated by the machine software. The velocity

time response of each sample was summed and averaged and is shown in Fig. 3a. The length of the energy absorbers varied from 10mm to 15mm, the latter value being the upper limit due to the energy capacity restrictions of the machine. Prior to each test conducted on each sample, the drop height parameter was set to zero before specifying an energy absorption value. This was done by adjusting the striker to be just touching the tip of each sample. Once the energy absorption value was specified, the machine automatically adjusted the striker to its appropriate height. For each sample tested, the data from the transducer was collected at a frequency of 5000Hz and a total of 100 data points were collected. The video recorder was mounted on a tripod and adjusted until a good viewing range was detected. In order to improve the quality of the video image, a black neutral material was placed behind the samples. In doing so, a clearer contrast of the sample image was achieved.

3.2. Preparation of the Oblong Tube Samples.

The Oblong tubes were formed by applying a tensile force to selected tubes, as shown in Fig. 3b. A tension displacement of 50mm was applied to the larger 127mm O.D., tube, thereby giving a ratio of 2.54, since the ratio is the O.D. of the tube divided by the tensile displacement length. This same ratio was used to calculate the displacement that needed to be applied to the remaining 101.6mm and 76.2mm O.D. tubes. In doing so, a constant displacement ratio was applied to each tube. Fig. 3c. presents the force - deflection response for each of the different sized tubes as a result of using this fixture.

4.0 Experimental Results and Discussion.

4.1. Analysis of the Oblong In Plane Standard System (OIPSS).

The various responses of an OIPSS (Oblong In-Plane Standard System) represented by three samples is shown in Fig. 4. For this system, the initial gaps between the three tubes have increased from 17mm and 19mm to 28mm and 56mm respectively due to the tension method used to create the oblong tubes. An increase in the displacement stroke was possible since the tubes have been elongated in the vertical direction. Therefore, it can be seen that the specific energy absorption of this kind of system will increase due the available increase in displacement stroke. Examining sample 1 from Fig. 4b it can be seen how the force rised abruptly as each successive tube established contact. Once this rise in force reached its peak (the collapse load of each tube has been reached), there existed a reduction in force or a softening stage. The reason for this behaviour was due to the fact that since the tubes have been plastically elongated in the vertical direction, the radius of curvature has reduced on the top and bottom hinge points of each tube. Therefore, the contact between the rigid platen and the outer tube can be approximated as a

‘point’ load application as demonstrated by Shim and Stronge [20]. This created a greater moment arm from the point of load application to the horizontal hinge points of each tube and, as a result, less force was required to maintain the deformation; hence a geometrical softening stage occurred. This phenomena was also observed by Morris et al [21] during the static compression of equivalent systems. Fig. 4c illustrates the energy - time response for such a system. It is clear how the curve can be approximated by three separate stages, each one representing the energy absorption of the outer, central and inner tubes respectively. Note how only partial displacement is achieved (see Fig. 4d) with this particular system. This is due to the maximum energy capacity that can be exerted by the impact tester. Therefore, it can be assumed that an extra displacement of 40mm would be achieved using a larger capacity machine.

4.2. Analysis of the Oblong In Plane Damped System (OIPDS).

The various responses of an OIPDS (Oblong In-Plane Damped System) are shown in Fig. 5. In an attempt to achieve a smoother force-deflection response than that exhibited by an OIPSS (Fig. 4a), two cylindrical spacers were used and inserted between the tubes as illustrated in by a schematic in Fig. 2c. From this, it can be clearly seen that once the moving mass impinges on this absorber, the three tube components will begin to deform synchronously. It should be noted that in order for the spacers to remain in position during the displacement stroke and to maintain symmetry, a mild steel dowel was placed through the machined holes of the upper portions of the tubes and the two spacers. A spot weld was used to fuse both ends of the dowel to the absorber. This approach was also used by Morris et al [21] for the static testing of circular tube type energy absorbers and it was found that symmetry was preserved for the complete displacement stroke and thereby a stable force deflection response was obtained. However, upon observation of sample 9 in Fig. 5d, it can be seen that symmetry was not achieved. Instead the spacers had a tendency to shift in the direction which offered the least resistance. It appears that the response is more sensitive to geometrical imperfections compared to its circular counterpart as noted in [21]. A possible reason for this increased sensitivity may be due to the fact that there is a greater chance of each tube deforming in an asymmetric manner due to the increased displacement stroke that must be undergone by the system. Also, due to the oblong shape of the tubes and the assemblage of the spacers with a steel dowel, it was difficult to achieve perfect symmetry before any loading was applied. This can also be regarded as a contributing factor in the observed behaviour of the system. Again this behaviour was also observed by Morris [21] for the static testing of such systems. The softening behaviour of this system (see

Fig. 5b) can also be explained using the concept of moment arms as previously described for the OIPSS section 4.1

5.0. Development and Analysis of the Finite Element Models.

5.1 Finite Element Modelling.

The explicit non linear finite element code LS-DYNA was used to predict the response of the aforementioned energy absorbers subjected to a free falling impinging mass. The complete model consisted principally of the striker, the assemblage of tubes and the base. These three components were modelled with an explicit structural solid consisting of eight nodes having translations, velocities and accelerations in the x, y and z directions at each node. The striker was modelled as a rigid entity with a translational displacement permitted in the vertical y direction, all other rotations and translations being fixed. In the material model, the mass density was increased to represent the total mass of both the carriage and the striker. For each of the two different absorbers analysed experimentally, an average velocity time curve was obtained and applied to the striker for the two different modelling cases. The base was modelled as rigid with all rotations and translations defined as fixed entities. The tubes contained within the two various energy absorbers were discretized by fully integrated solid elements. Although this type of formulation leads to an increase in CPU time, the undesirable feature of hour glassing was avoided.

The OIPDS was also modelled with shell elements in order to make a comparison of results against the system represented by brick elements. This shell model was represented by the Belytschko-Tsay shell element with five integration points defined through the thickness of each tube. Symmetry conditions were invoked along the appropriate symmetry planes in order to reduce CPU time. The striker was also modelled as a rigid entity using brick elements as described in the preceding paragraph.

5.2. Mesh Convergence.

Fig. 6a. illustrates the convergence plot of three different mesh densities. It can be seen that a convergence solution was achieved when five or six brick elements were used to mesh the thickness of the tubes. Hence all subsequent models involving brick elements consisted of a mesh density involving five bricks through the thickness of each tube. Accordingly, a force - time plot of the OIPDS illustrating the response for three, five and six elements through the thickness of each tube is illustrated in Fig. 6b. For the shell models, a convergence study was also undertaken with Fig. 7a. illustrating the force - time

response of three different mesh densities. Three simulations with a shell element length of 4mm, 2mm and 1mm were conducted.

The contact algorithm used to simulate contact between the respective components (striker, tubes and base) was based on the 'Automatic Surface to Surface Contact' algorithm in which contact was established when a surface of one body penetrates the surface of another body. This contact algorithm was used for both the brick and shell element models. A static coefficient of friction value of 0.2 was assigned to the contact pairs to prevent lateral movement between the respective tubes.

5.3. Geometry Creation of the Oblong Shaped Tubes.

To obtain the new geometry profile of the oblong shaped tubes, appropriate loading and boundary conditions as observed in experiment were applied to the circular tubes in the finite model. This was achieved using the implicit finite element code via ANSYS. Prescribed vertical displacements of 50mm, 40mm and 30mm were applied to the outer, central and inner tubes respectively using three individual pilot nodes. An inlay in Fig. 8a illustrates this method. Numerical and experimental comparison for the response of the tubes subjected to tensile displacement is also presented in this figure. Once the full displacement was applied, the three tubes were unloaded until the force ramped back to zero. This was done in order to take into account the final state of deformation due the elastic spring back which occurred when the tensile load was removed. The final geometric profile was updated from the deformed mesh using update geometry capabilities in ANSYS before being imported into LS-DYNA for further pre-processing and solution.

5.4. Material Characterisation.

For material characterisation of the tubes, a bilinear stress–strain curve was incorporated into the finite element model using the 'PLASTIC KINEMATIC HARDENING' material model option. Values of 0.3 and 200 GPa were given for Poisson's ratio and Young's modulus respectively. The material is assumed to possess only isotropic strain hardening and strain rate effects due to dynamic loading are defined using the Cowper-Symonds constitutive equation given by

$$\sigma_d = \sigma_s \left(1 + \left[\frac{\dot{\varepsilon}}{D} \right]^{\frac{1}{q}} \right) \tag{1}$$

where σ_d is the dynamic flow stress at a uniaxial plastic strain rate $\dot{\varepsilon}$, σ_s is the associated static flow stress, the material constants given for D and q were given as 6844 and 3.91 respectively. These values were used in previous studies for the axial crushing of mild steel tubes and dynamic loading [22].The values for the yield stress and plastic modulus as outlined in section 2.4 were incorporated into this material model.

6.0. Numerical Results and discussion.

6.1. Energy Balance.

To ensure that there were no numerical errors within the developed models to simulate the various energy absorbers, the energy equation was checked to ensure that it was in a balanced state. The following energy equation must hold true at all times during an analysis and is given by [23] -

$$E_{kin} + E_{\text{int}} + E_{si} + E_{rw} + E_{damp} + E_{hg} = E^0_{kin} + E^0_{\text{int}} + E_{ext}$$

where on the left hand side E_{kin} is the kinetic energy, E_{int} the internal energy, E_{si} the sliding energy (friction energy), E_{rw} rigid wall energy, E_{damp} is energy due to damping and E_{hg} hourglass energy, on the right hand side $E^0_{kin}, E^0_{\text{int}}, E_{ext}$ are energies due to initial kinetic, initial internal and external work done respectively. Since the models in question only contain kinetic, internal and sliding energy and external work done on the system, the energy balance reduces to

$$E_{kin} + E_{\text{int}} + E_{si} = E_{ext}$$

The terms on the left hand side is equivalent to the total energy. Hence, it can be seen from Fig. 9c and Fig. 10c that the energy condition for each model is in a balanced state indicating that no energy been introduced or absorbed artificially that may be generated due to numerical instability.

6.2. Evaluation of the OIPSS and OIPDS. (Brick Element Models)

For the OIPSS and OIPDS, the force and energy responses are over-predicted by the numerical code. Values of 32% and 40% in the over estimation of energy absorption are observed as shown in Fig. 9b and Fig. 10b respectively. There appears to be two reasons for the over-prediction in results illustrated by the numerical method. Upon analysis of the OIPDS (See Fig. 11a), it can be seen from an experimental point of view that both the static and dynamic cases exhibit similar force deflection response in terms of magnitude. This would indicate for the given velocity applied to the striker, that the strain rate sensitivity

is not a significant factor in the deformation response of this particular system. From a numerical standpoint, in which the effects of strain rate were both included and excluded, it can be seen that the force magnitude was over-predicted in both cases. With the aid of examining the strain rate sensitive numerical response from Fig. 11a, it appears the first reason for the over-prediction in force is due to the values of D and q used in the Cowper-Symonds relation. These values may not be valid in this particular application since an obvious large increase in the dynamic yield stress is evident using the specified strain rate parameters, where in fact, both the experimental static and dynamic results show similar forces of magnitude. The usual constants of 40.4 and 5 for D and q are normally used by researchers; however, it was found that substitution of these values into the Cowper-Symond relation yields an even larger value of yield stress than the constants of 6844 and 3.91 used in the current material model. The constants of 40.4 and 5 have also have been used by [24] to predict the dynamic force magnitude for the internal inversion of mild steel tubes. It was found that the dynamic load conditions greatly over-predicted those that were recorded experimentally. It appears that the constants only apply to applications involving small strains (5%) and not to large strains that are encountered in the internal inversion of mild steel tubes. Large strains also exist in the lateral compression of the aforementioned tube systems. Therefore, it is apparent that more research needs to be conducted in this area in terms of obtaining experimental data pertaining to material strain rate sensitivity of mild steel. Such experimental data needs to be collected in the form of a range of constants which represent the behaviour of mild steel at different strain rates and strain levels [25].

The second reason for the over-prediction appears to be in the difficulty of the numerical code to accurately predict where the horizontal hinge points (collapse points) should occur in order for the tubes to collapse plastically. By examining the initial stages of displacement in Fig. 11b, one could visualise each tube within this oblong shaped absorber to consist of two arcs at the top and bottom joined together by two separate columns. In doing so there is the possibility that the numerical code predicts the plastic collapse hinges to occur elsewhere, possibly in the regions of point A , B (See Fig. 11b) due to the fact that the central portion of the tube is acting like a column. This ‘column effect’ is known experimentally to strengthen the load capacity of an elliptical tube due to its stiffness when compressed between rigid platens [19].Therefore, in view of this, when the striker impinged on the upper portion of this energy absorber, a rapid rise in reactive force was observed due to this ‘column effect’. In order to support this explanation for the discrepancy, a CIPDS (Circular In-Plane Damped System) was designed and

modelled using brick elements as shown in Fig. 12b and validated using experimental techniques. This particular system was compressed quasi-statically and hence the simulation model was solved using the implicit version of the finite element code. From Fig. 12a, it can be seen that there is a very good correlation between the experimentally observed force-deflection response and that obtained from the numerical model. This implies that the location of the plastic hinges in each circular tube throughout the compression stroke was adequately captured by the numerical code. It should be noted that the same yield stress and initial plastic modulus was incorporated into this numerical model as outlined in section 2.4.

6.3 Evaluation of the OIPDS. (Shell Element Model)

Fig. 13a illustrates a comparison of results between the shell element model and the actual experimentally observed force-deflection response. The same procedure as described in the preceding paragraph was employed in which the OIPDS was simulated with and without the strain-rate effects. It can be seen that with the inclusion of strain rate effects, the collapse load appears to be well over predicted and it should be noted that the magnitude of force is similar to that of its brick element counterpart. However, in the post collapse stages, the force reduces considerably indicating the ability of the shell element to more accurately predict the force due to this bending dominated mode of deformation. For the shell model and excluding the effects of strain rates sensitivity, it can be seen that there is quite a good correlation between the numerical and experimental result. The collapse load is still over estimated although the magnitude is considerably less than its corresponding brick model counterpart as shown in Fig. 11a. It appears that the shell element model also has difficulty to correctly predict the collapse load for this OIPDS: it may be due to the straight portion of the oblong tubes acting as columns as outlined in section 6.2. For an interesting comparison, Fig. 13c is displayed which offers a comparison of results between the shell and brick element formulations and that of experiment. It appears that the shell element formulation is the better one to use since it is quite suited to model bending dominated problems. In addition to this, the solution time using the shell element formulation is considerably less than that when using the brick element formulation.

7.0. Conclusion.

An experimental program has been reported describing the procedure in setting up the impact tester for the dynamic lateral compression of two types of oblong energy absorbers, namely the OIPSS and the OIPDS. A description was given on how initially circular tubes were formed into oblong tubes with the aid of a simple custom designed fixture. The advantage of such tubes is that the displacement stroke can

be increased which automatically increases its specific energy absorbing capacity. A brief description was given on how the concept of moment arms causes a structure to harden or soften geometrically depending on whether this moment arm increases or reduces in length. This change in length depends on the type of loading geometry applied such as point load indenter or a flat plate indenter.

Concurrent to the experimental work, results of explicit non linear finite element simulation using LS-DYNA to simulate the dynamic crushing of the various absorbers using both brick and shell elements was presented. The boundary conditions of the numerical models were subjected to the same test conditions as observed in the experimental program. An attempt was made to explain why large discrepancies existed between the experimental and the numerical method particularly for the brick element models. A numerical energy balance was examined on each model to ensure that no artificial energy was introduced to confirm that no numerical errors were present. A more in depth numerical analysis may be required in the modelling of the columns in order to accurately predict the force-deflection response due to the 'column effect' present in the OPISS and OIPDS. In addition to this, the resulting initial stress field generated as a consequence of the oblong shaping process may play a part in the initial stress state of each oblong tube before any compression load is applied. Hence, a numerical model containing the initial stress field as a result of this shaping process may play a part in the final result of the numerical simulations.

Despite the over-predictions exhibited by the numerical code, particularly with the application of brick elements, an optimised force deflection response has been obtained. The optimised energy absorber (OIPDS) is seen as an improvement on the OIPSS since the insertion of cylindrical rods caused the crushing force to be relatively constant once the collapse load has been reached, which is a desirable feature in the design of energy absorbers.

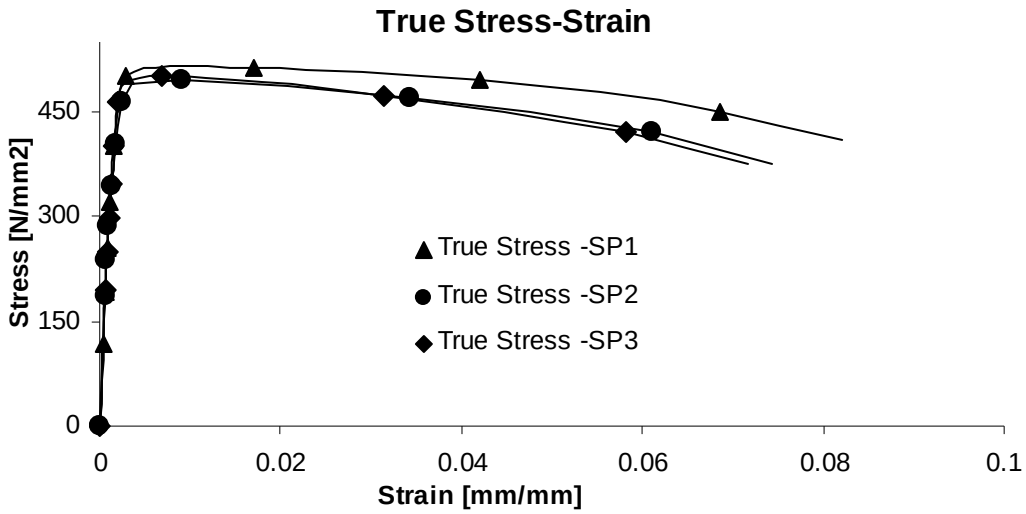

(a)

Fig. 1. (a) A true stress - strain curve obtained from three tensile specimens.

(a)

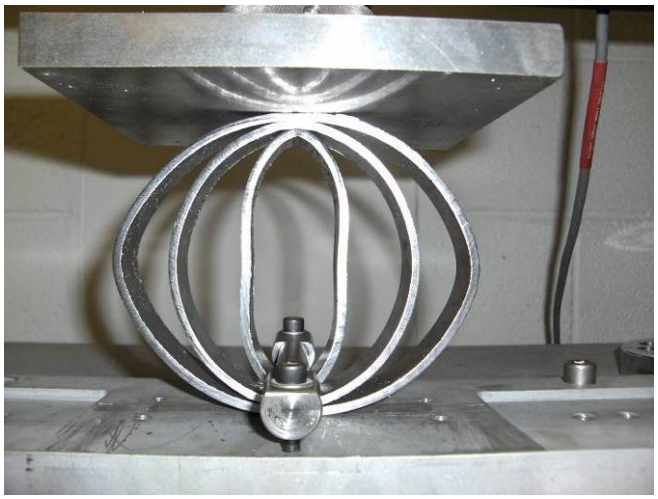

(b)

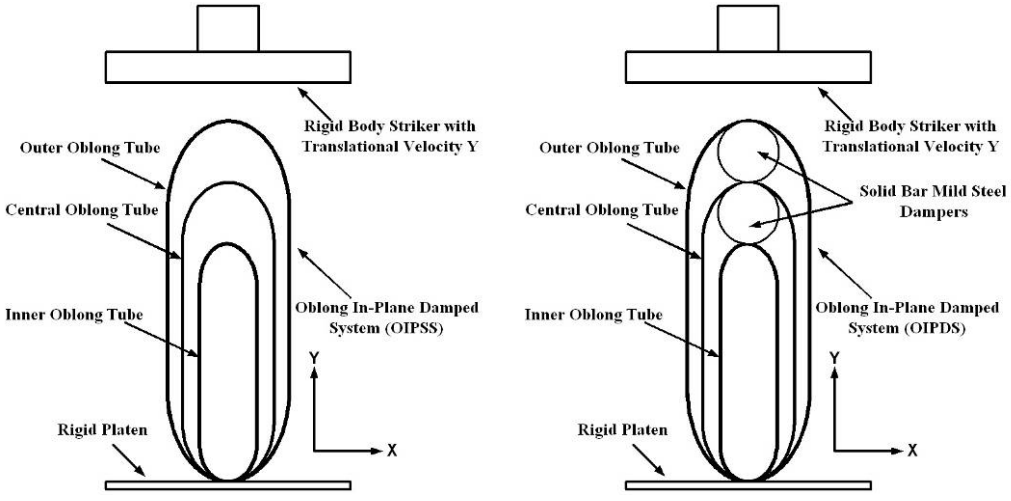

(c)

Fig. 2. (a) The Zwick Roell impact machine used to conduct the experiments.
(b) The fixture used to hold the samples in place upon impact.
(c) A schematic of both the OIPSS and the OIPDS.

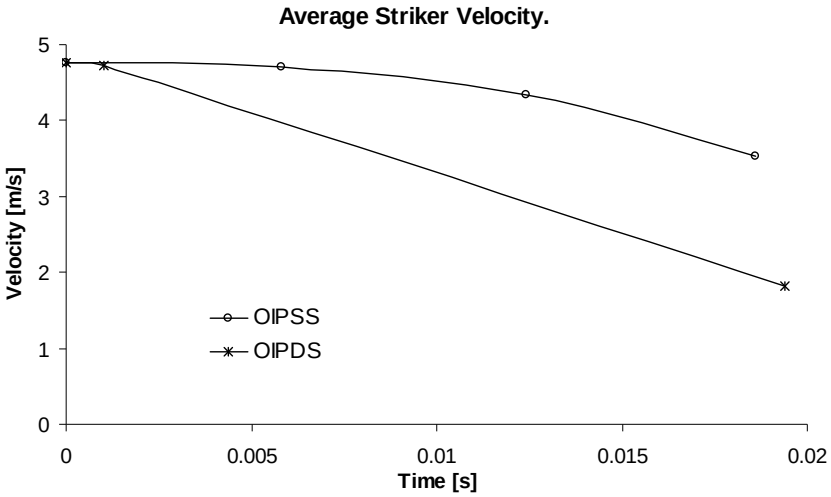

(a)

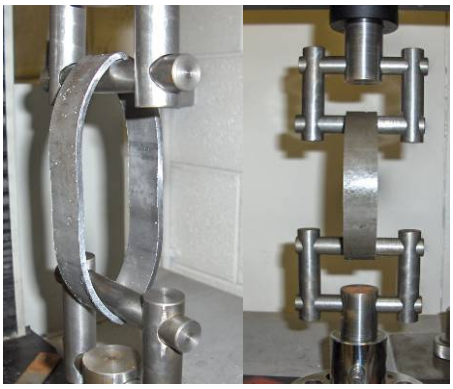

(b)

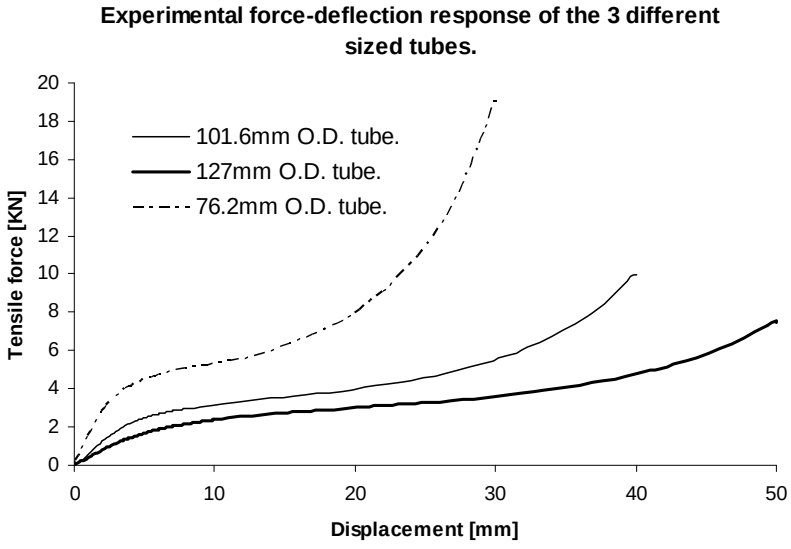

(c)

Fig. 3. (a) The average striker velocity applied to the respective samples.
(b) The fixture used to elongate the circular tubes into an oblong shape.
(c) Tensile force - deflection response of the three individual tubes.

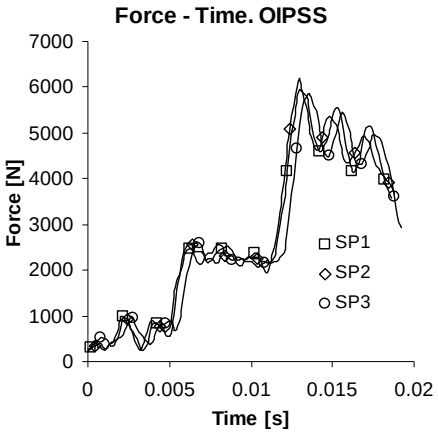

(a)

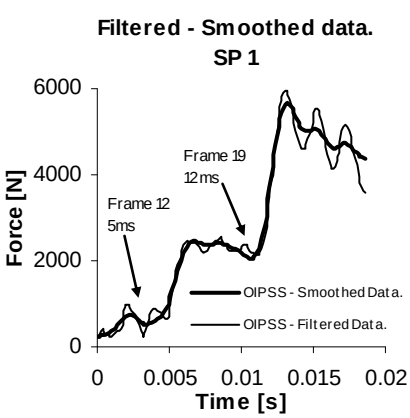

(b)

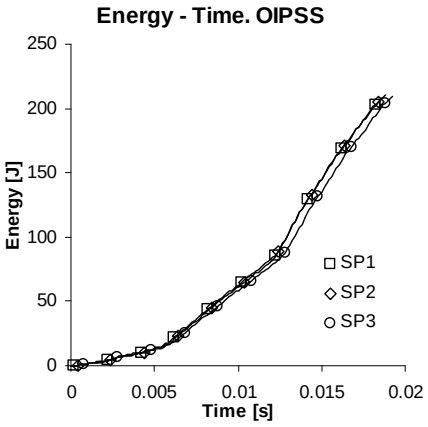

(c)

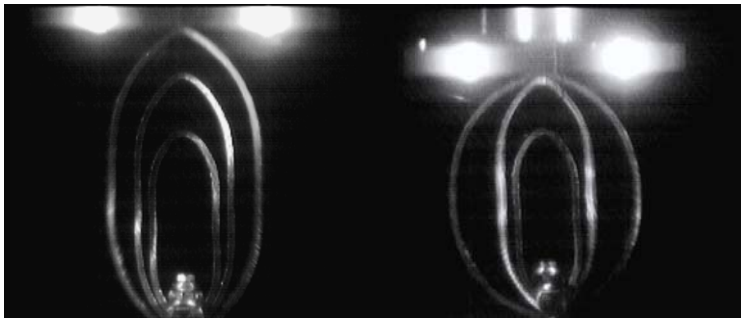

Frame 1: 0ms. Frame 12: 5ms.

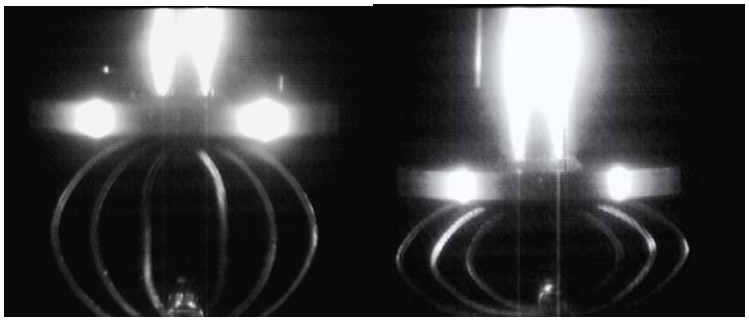

(d) Frame 19: 12ms. Frame 29: 19ms

Fig. 4. (a) Force time curve for an OIPSS.
(b) Sample 1: Filtered - Smoothed data.
(c) Energy time response for an OIPSS.
(d) Experimental displacement evolution of sample 1.

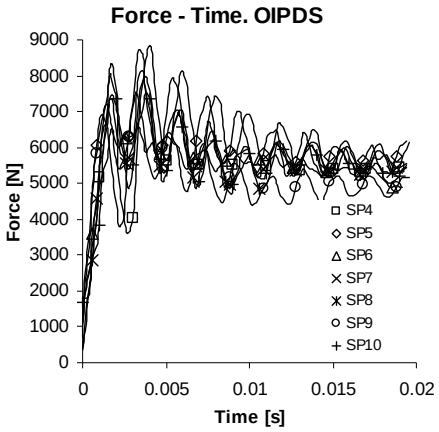

(a)

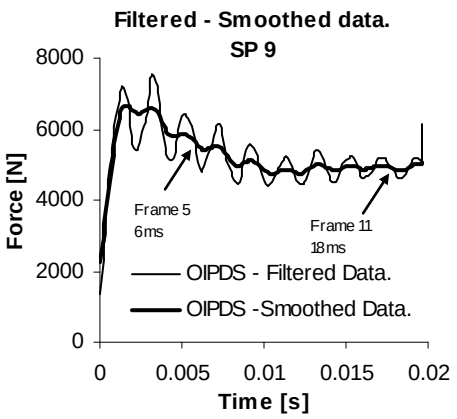

(b)

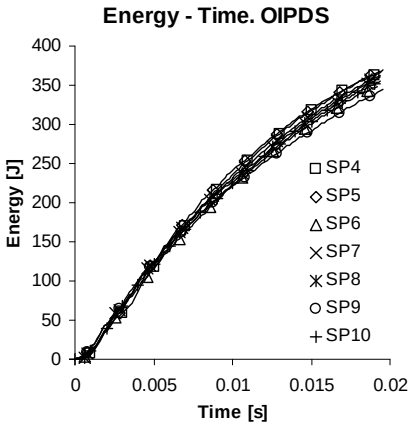

(c)

Frame 1: 0ms. Frame 5: 6ms.

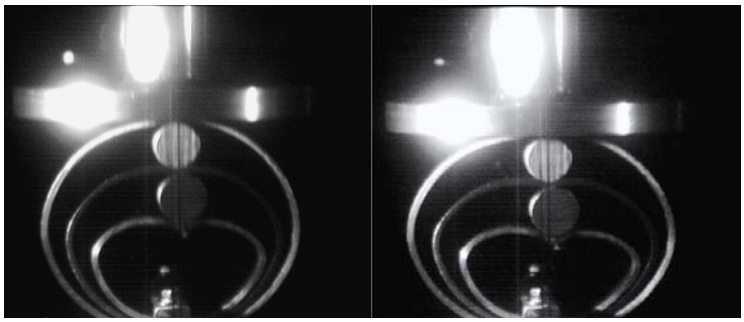

(d) Frame 11: 18ms. Frame 15: 20ms.

Fig. 5. (a) Force time curve for an OIPDS.
(b) Sample 9: Filtered-Smoothed data.
(c) Energy time response for an OIPDS.
(d) Experimental displacement evolution of sample 9.

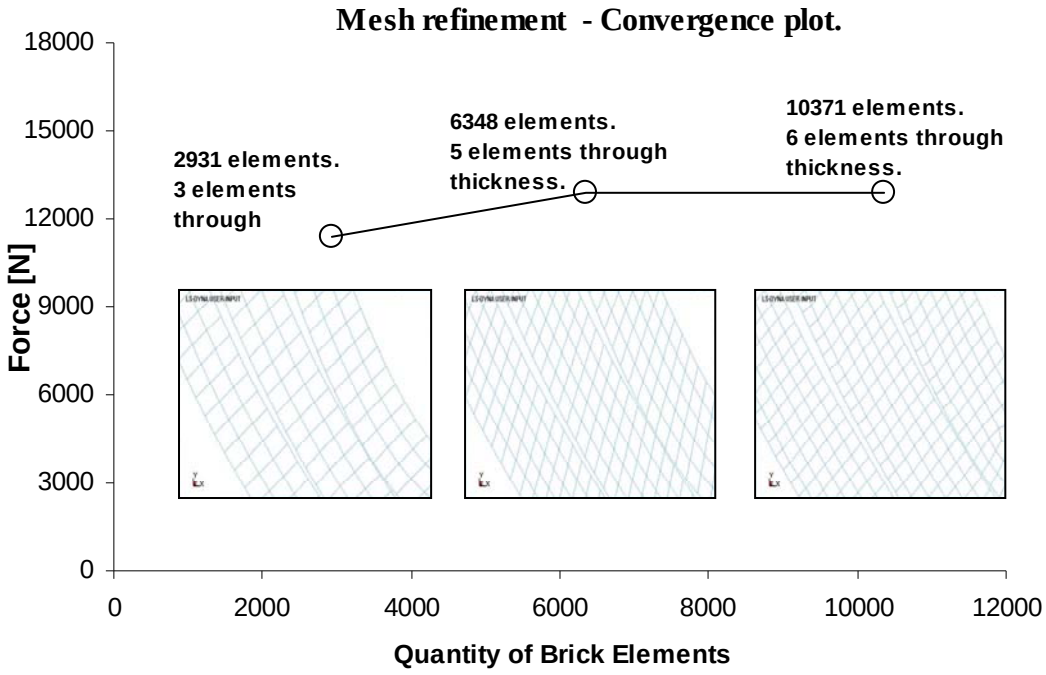

(a)

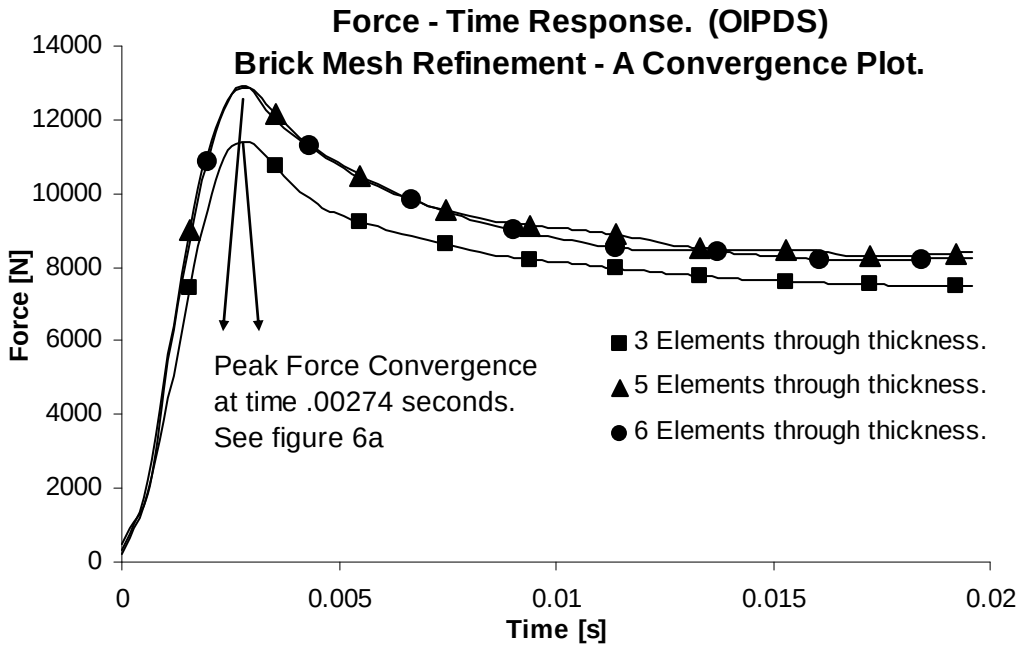

(b)

Fig. 6. (a) A convergence plot illustrating the number of brick elements for each of the three different mesh densities.
(b) A force-time convergence plot of the OIPDS analysed with 3, 5 and 6 brick elements through the thickness of each tube.

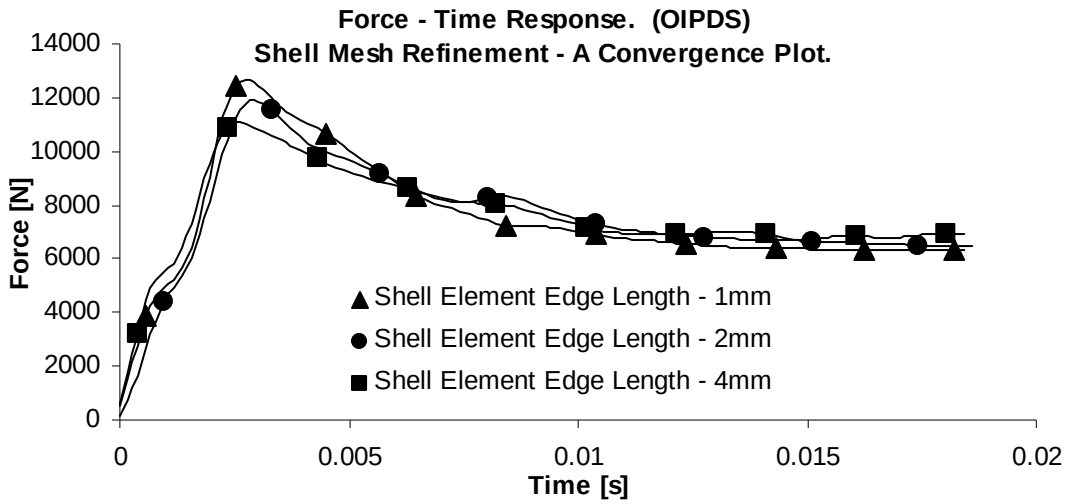

(a)

Fig. 7. (a) A force - time convergence plot of the OIPDS analysed with five integration points through the thickness of each tube.

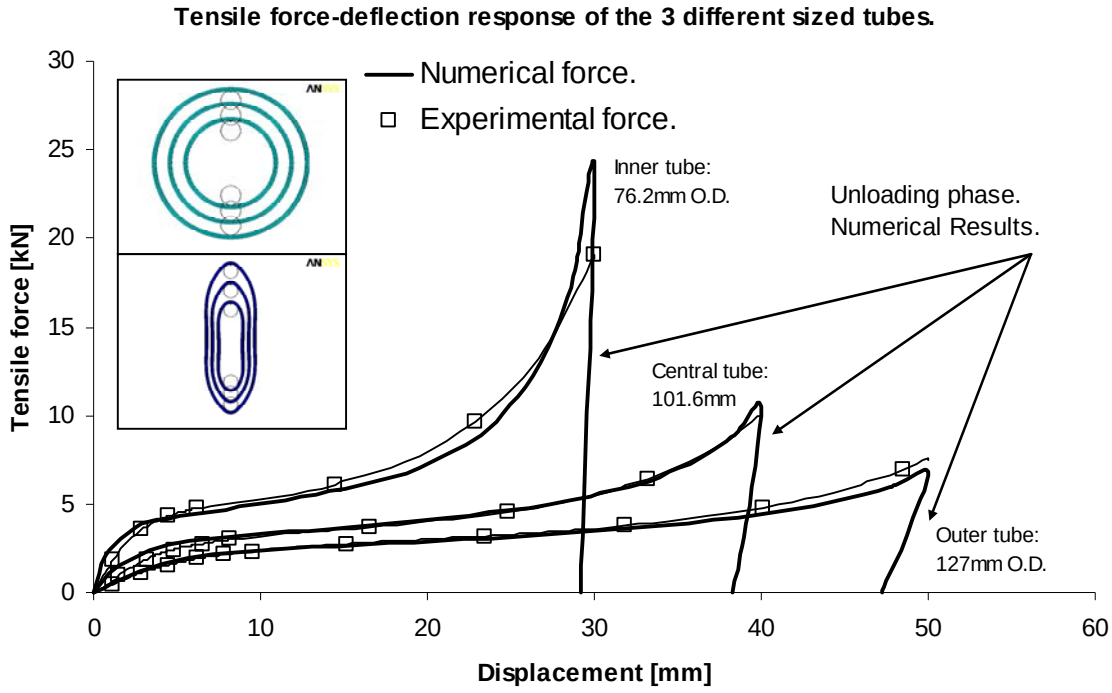

(a)

Fig. 8. (a) A comparison of the numerical (brick model) and experimental tensile force - deflection response of the three tubes used in the various energy absorbers.

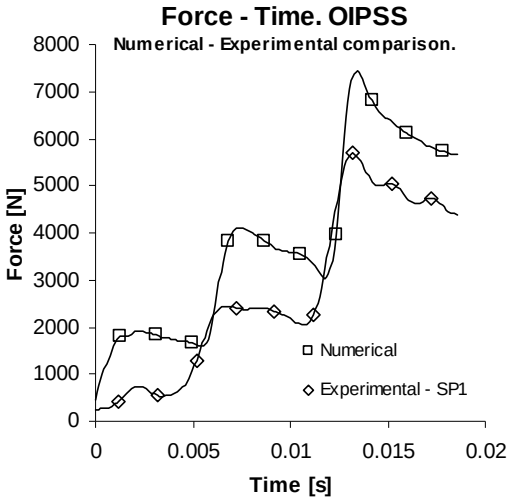

(a)

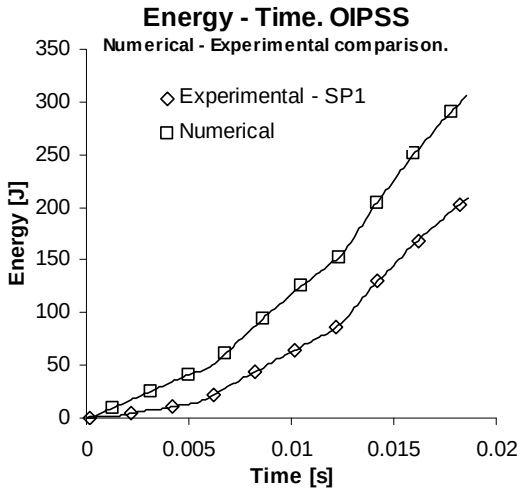

(b)

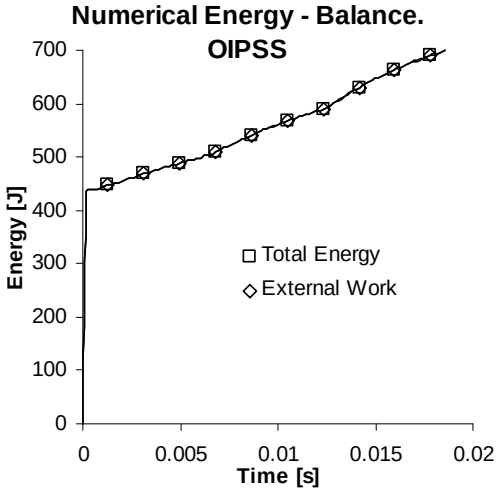

(c)

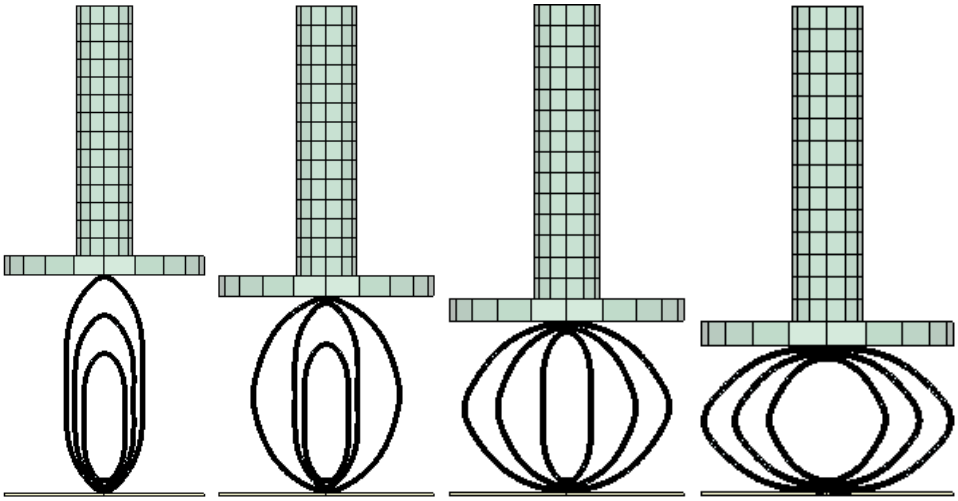

(d)

Fig. 9. (a) Force - time curve for an OIPSS displaying the numerical (brick model) and the smoothed experimental force-deflection response.
(b) Numerical (brick model) and experimental comparison of the energy - time response for an OIPSS.
(c) Numerical energy balance of the total work and external work on the system.
(d) Numerical plot of the displacement evolution for an OIPSS.

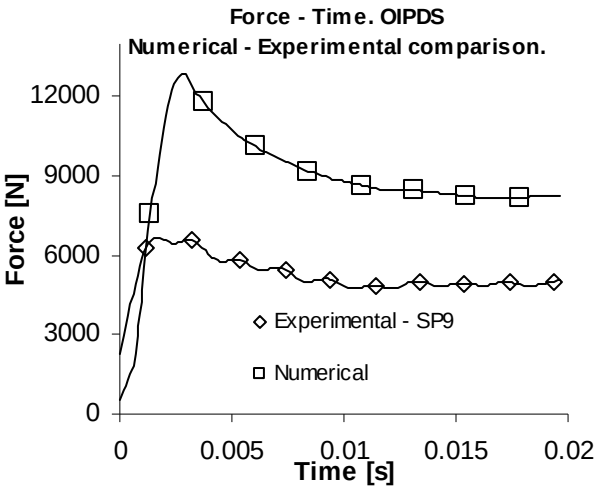

(a)

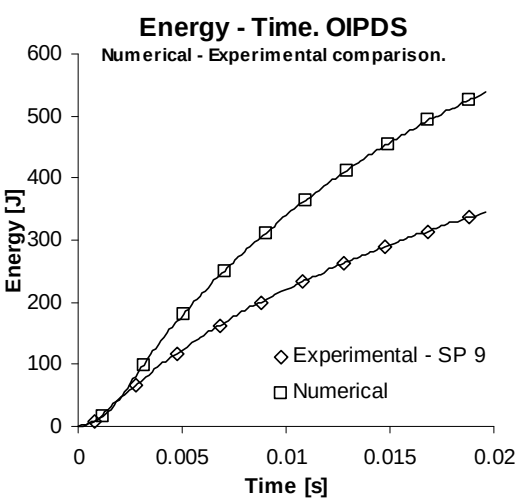

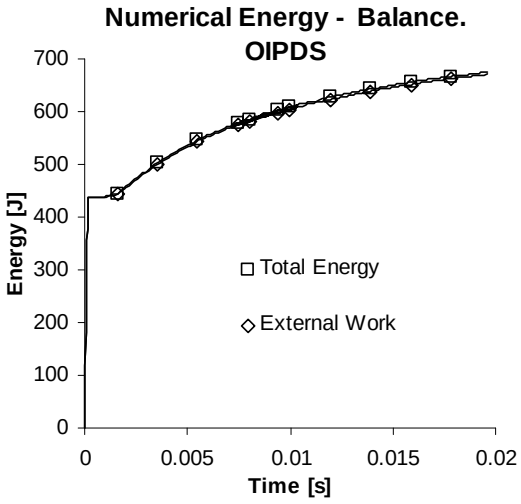

(b) **(c)**

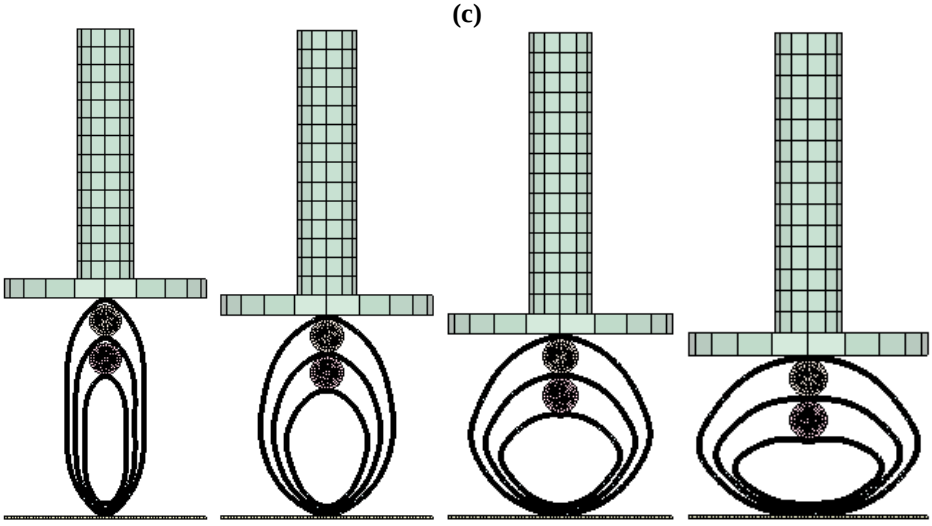

(d)

Fig. 10. (a) Force - time curve for an OIPDS displaying the numerical (brick model) and the smoothed experimental force-deflection response.
(b) Numerical (brick model) and experimental comparison of the energy - time response for an OIPDS.
(c) Numerical energy balance of the total work and external work on the system.
(d) Numerical plot of the displacement evolution for a brick modelled OIPDS.

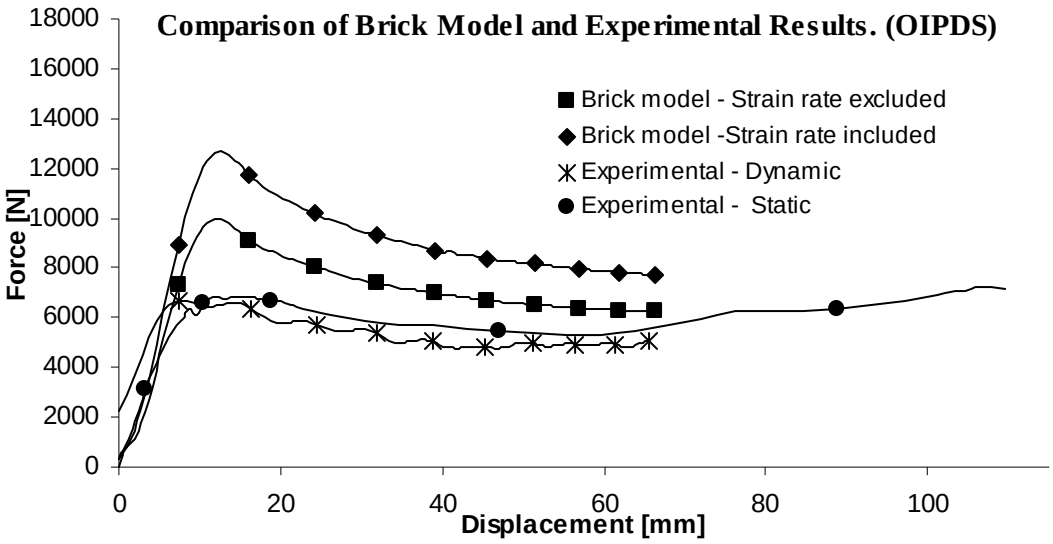

(a)

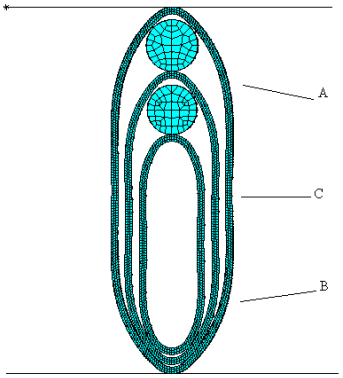

(b)

Fig. 11. (a) Comparison of a brick model with experimental results.
(b) Locations of the possible plastic hinges.

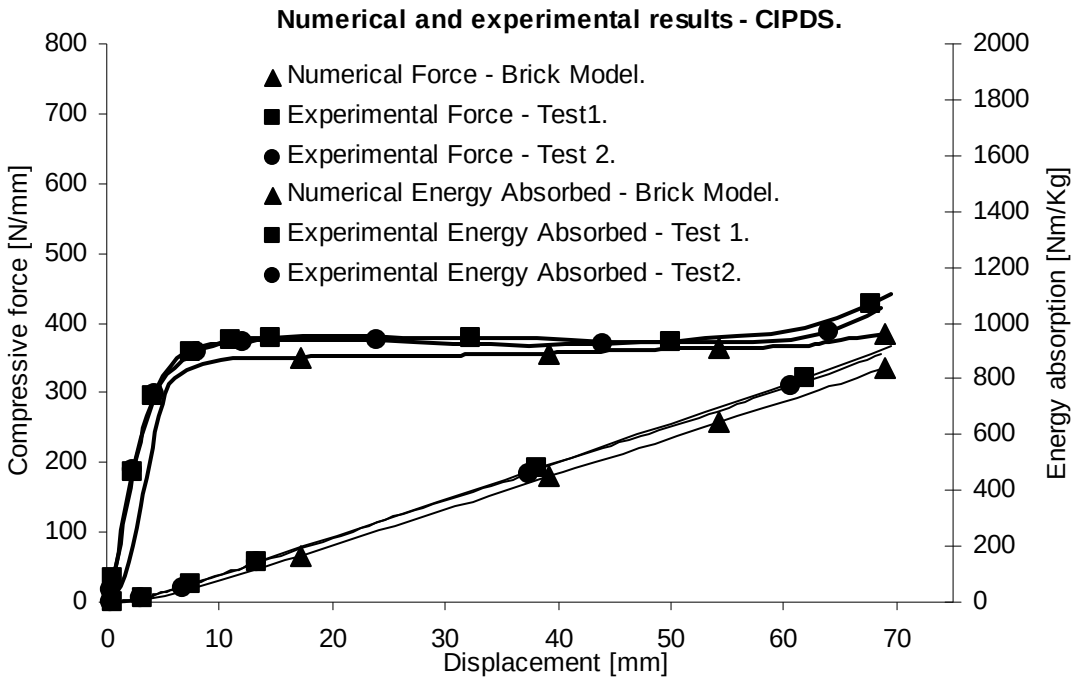

(a)

(b)

Fig. 12. (a) Experimental and numerical comparison of a CIPDS compressed under quasi-static conditions.
(b) A comparison of initial and final stages of displacement of a CIPDS produced by a digital camera and ANSYS.

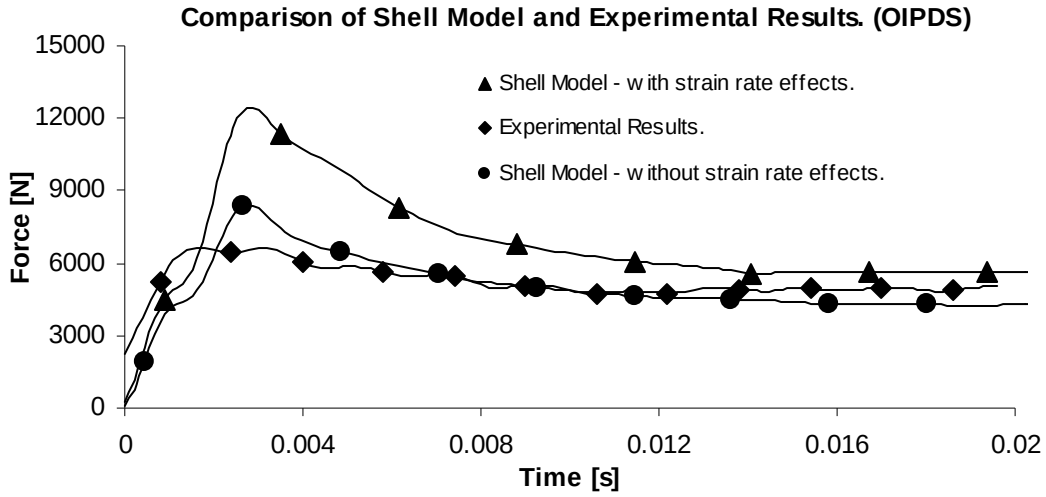

(a)

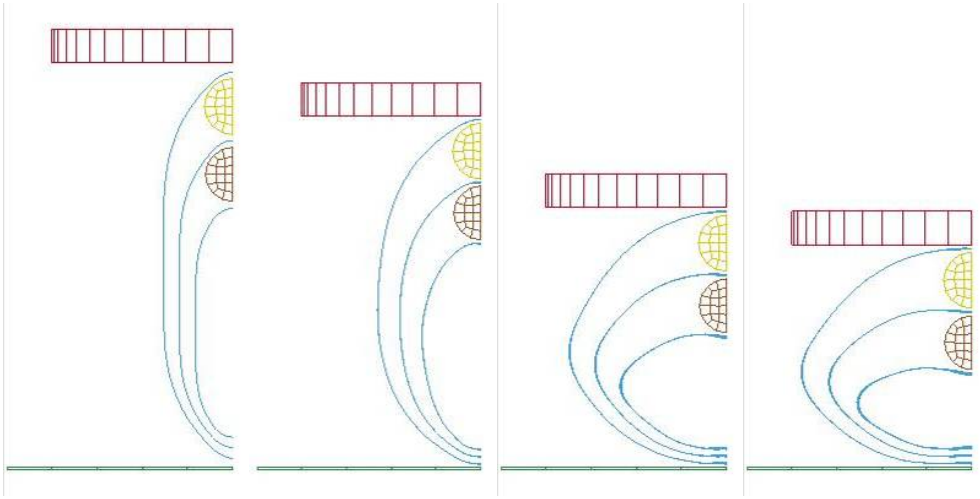

(b)

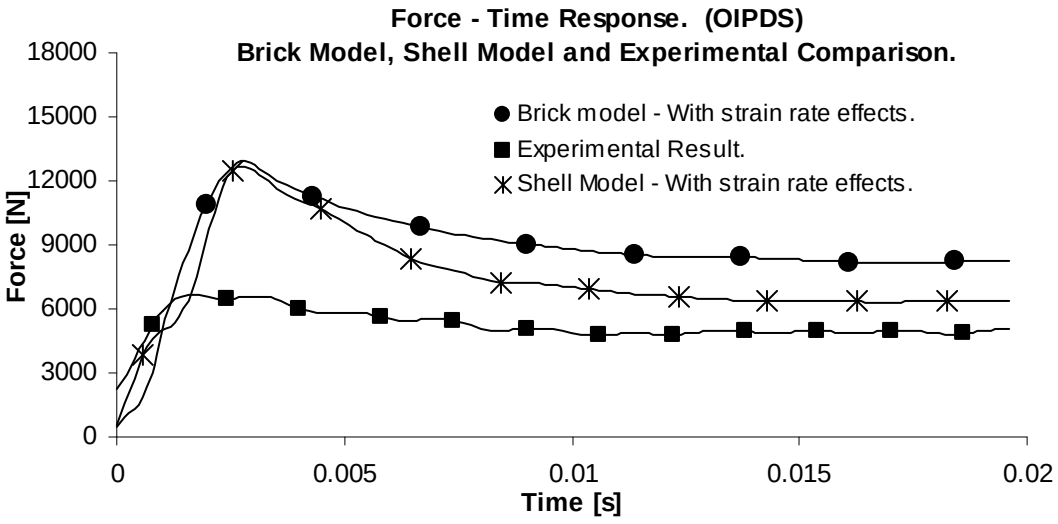

(c)

Fig. 13. (a) A force – time plot comparing the brick and shell model against the actual observed result for an OIPDS.
(b) Numerical plot of the displacement evolution for a shell modelled OIPDS.
(c) A force – time plot comparing the brick and shell model against the actual observed result for an OIPDS.

Table 1. Results obtained from experiments for the 10 samples tested.

	T_{final} (s)	$V_{initial}$ (mm/s)	V_{final} (mm/s)	Stroke (mm)	Energy (J)
OIPSS Length (10mm)					
SP1	0.0186	4.75	3.45	81	208
SP2	0.0188	4.76	3.50	82	210
SP3	0.0192	4.76	3.50	84	209
OIPDS Length (15mm)					
SP4	0.0196	4.76	1.62	63	369
SP5	0.0194	4.76	1.63	62	368
SP6	0.0192	4.74	1.90	64	349
SP7	0.0194	4.78	1.77	64	363
SP8	0.0194	4.78	1.82	64	360
SP9	0.0196	4.76	2.00	66	345
SP10	0.0194	4.75	1.84	64	355

References.

[1] Burton, R.H., Craig, J.M., "An Investigation into the Energy Absorbing Properties of Metal Tubes Loaded in the Transverse Direction. "1963, BSc (Eng) Report, University of Bristol, England.

[2] DeRuntz, J. A., Hodge, P. G., "Crushing of a Tube between Rigid Plates." Transactions of ASME, Journal of Applied Mechanics., 1963, 30:391-395.

[3] Redwood, R. G., "Discussion of Ref. 2." Transactions of ASME, Journal of Applied Mechanics., 1964, 31:357-358.

[4] Reid, S. R., Reddy, T. Y., "Effect of Strain Hardening on the Lateral Compression of Tubes between Rigid Plates. " Int J of Solids and Structures, 1978, 14 (3): 213-225.

[5] Avalle, M., Goglio, L., "Static Lateral Compression of Aluminium Tubes: Strain Gauge Measurements and Discussion of Theoretical Models." Journal of Strain Analysis., 1997, 32 (5):335-343.

[6] Reddy, T., Reid, S., "On Obtaining Material Properties from the Ring Compression Test." Nuclear Engineering and Design., 1979, 52:257-263.

[7] Gupta, N. K., Sekhon, G. S., Gupta, P. K., "Study of Lateral Compression of Round Metallic Tubes." Thin-Walled Structures, 2005, 43(6):895-922.

[8] Reid, S. R., Reddy, T. Y., "Experimental Investigation of Inertia Effects in One- Dimensional Metal Ring Systems Subjected to End Impact -- I. Fixed-Ended Systems," Int J of Impact Engng, 1983, 1(1):85-106.

[9] Reddy, T. Y., Reid, S. R., Barr, R., "Experimental Investigation of Inertia Effects in One-Dimensional Metal Ring Systems Subjected to End Impact--II. Free-Ended Systems," Int J of Impact Engng, 1991, 11(4):463-480.

[10] Johnson, W., Reid, S. R., Reddy, T. Y., "The Compression of Crossed Layers of Thin Tubes." Int J of Mech Sci, 1977, 19(7):423-428.

[11] Shrive, N., Andrews, K., England, G., "The Impact Energy Dissipation of Cylindrical Systems." Structural Impact and Crashworthiness. J. Morton, editor. Elsevier Applied Science Publishers. London, England, 1984. Vol 2: p. 544-554.

[12] Reddy, T., Reid, S., “Lateral Compression of Tubes and Tube-Systems with Side Constraints.” Int J Mech Sci 1979, 21(3): 187-199.

[13] Morris, E., Olabi, A., Hashmi, S., “FE Simulation and Experimentation of Nested Systems under Static and Impact Loading Conditions."In: Proceedings of the 12th International Conference on Experimental Mechanics. Bari, (Italy) 2004. p. 196-203.

[14] Morris, E., Olabi, A., Hashmi, S., "Post Collapse Response of Nested Tube Systems with Side Constraints." In: Vickery, J., editor. Proceedings of the 22nd International Manufacturing Conference. Tallaght, Dublin (Ireland) 2005. p. 693-700.

[15] Morris, E., Olabi, A., Hashmi, S., "Experimental and Numerical Analysis of the Static Lateral Compression of Tube Type Energy Absorbers with Different Indenters." The Engineers Journal, 2005. 59(8) p. 505 - 510.

[16] Morris, E., Olabi, A., Hashmi, S., "Plastic Response of Nested Systems under Static and Dynamic Loading Conditions using FE and Experimental Techniques. "In: Dulieu-Barton J., Quinn, S., editors. Proceedings of the 4th International Conference on Advances in Experimental Mechanics. Trans Tech Publications, 2005, Vol 3-4: p 377-382.

[17] Reid, S. R., Drew, S. L. K., Carney, I.J.F., "Energy Absorbing Capacities of Braced Metal Tubes," Int J of Mech Sci, 1983, 25(9-10):649-667.

[18] Wu, L., Carney III, J. F., "Initial Collapse of Braced Elliptical Tubes under Lateral Compression," Int J of Mech Sci, 1997, 39(9):1023-1036.

[19] Wu, L., Carney III, J. F., "Experimental Analyses of Collapse Behaviours of Braced Elliptical Tubes under Lateral Compression," Int J of Mech Sci, 1998, 40(8):761-777.

[20] Shim, V. P., Stronge, W. J., "Lateral Crushing of Thin-Walled Tubes between Cylindrical Indenters," Int J of Mech Sci, 1986, 28(10):683-707.

[21] Morris, E., Olabi, A., Hashmi, S., “The quasi-static analysis of nested circular and oblong tube energy absorbers subjected to lateral deformation.” 2006, Submitted for review to the Int J of Mech Sci.

[22] Nagel, G., Thambiratnam, D., “A numerical Study on the Impact Response and Energy Absorption of Tapered Thin-Walled Tubes”. Int J of Mech Sci. 2004, 46(2):201-216.

[23] LS-Dyna Theoretical Manual, Livermore Software Technology Corporation: Livermore, California; May 1998.

[24] Harrigan, J. J., Reid, S. R., Peng, C., "Inertia Effects in Impact Energy Absorbing Materials and Structures," Int J of Impact Engng, 1999, 22(9-10):955-979.

[25] Abramowicz, W., Jones, N., "Dynamic Progressive Buckling of Circular and Square Tubes," Int J of Impact Engng, 1986, 4(4):243-270.